Optics Letters

Clamp-type quartz tuning fork enhanced photoacoustic spectroscopy

Qian Wu,[1] Haohua Lv,[1] Leqing Lin,[1] Hongpeng Wu,[2] Marilena Giglio,[3] Wenguo Zhu,[1] Yongchun Zhong,[1] Angelo Sampaolo,[3] Pietro Patimisco,[3] Lei Dong,[2,4] Vincenzo Spagnolo,[3] Jianhui Yu,[1] and Huadan Zheng[1,*]

[1]Guangdong Provincial Key Laboratory of Optical Fiber Sensing and Communications, and Department of Optoelectronic Engineering, Jinan University, Guangzhou, 510632, China
[2]State Key Laboratory of Quantum Optics and Quantum Optics Devices, Institute of Laser Spectroscopy, Shanxi University, Taiyuan 030006, China
[3]PolySense Lab, Dipartimento Interateneo di Fisica, University and Politecnico of Bari, CNR-IFN, Via Amendola 173, Bari 70126, Italy
[4]e-mail: donglei@sxu.edu.cn
*Corresponding author: zhenghuadan@jnu.edu.cn

Received 20 May 2022; revised 16 June 2022; accepted 26 July 2022; posted 5 August 2022; published 31 August 2022

In this Letter, clamp-type quartz tuning fork enhanced photoacoustic spectroscopy (Clamp-type QEPAS) is proposed and realized through the design, realization, and testing of clamp-type quartz tuning forks (QTFs) for photoacoustic gas sensing. The clamp-type QTF provides a wavefront-shaped aperture with a diameter up to 1 mm, while keeping Q factors > 10^4. This novel, to the best of our knowledge, design results in a more than ten times increase in the area available for laser beam focusing for the QEPAS technique with respect to a standard QTF. The wavefront-shaped clamp-type prongs effectively improve the acoustic wave coupling efficiency. The possibility to implement a micro-resonator system for clamp-type QTF is also investigated. A signal-to-noise enhancement of ~30 times has been obtained with a single-tube acoustic micro resonator length of 8 mm, ~20% shorter than the dual-tube micro-resonator employed in a conventional QEPAS system.

https://doi.org/10.1364/OL.464334

Photoacoustic spectroscopy (PAS) is a powerful technique for trace gas detection in environmental monitoring, medical diagnosis, and industrial applications [1,2]. When modulated laser light resonant with an absorption line of a target gas species is shone on a sample containing it, part of the optical energy is absorbed, exciting the gas target molecules from their ground states. The de-excitations of these molecules occur via vibration-translation (V-T) relaxation channels, which leads to a modulated heating of the gas sample and subsequently to the generation of pressure waves [3]. Compared with other optical sensing technologies, no optical detector is required in PAS, since an acoustic transducer can convert the pressure waves into electrical signals [4–9]. Another unique advantage of PAS is that the PA signal does not rely on the optical absorption length and thereby sensitive detection can be achieved with compact and robust sensor architectures.

The PAS signal amplitude S shows a $S \propto a \cdot P$ relationship, where a is the molecular absorption line intensity and P is the excitation optical power [10]. Since the strongest molecular absorption lines lie in the mid-infrared (MIR) and THz regions (typically a few orders stronger than that in the near-infrared region), the PAS sensitivity can be greatly enhanced by exploiting laser sources operating in the MIR to THz such as optical frequency comb, and interband- and quantum-cascade lasers (ICLs and QCLs) [11–13]. Implementing high power optical sources further boosts the PAS sensitivity, and parts-per-trillion concentration detection levels or normalized noise equivalent absorption coefficients down to 10^{-11} W/cm/Hz$^{1/2}$ can be achieved [14–16].

Quartz enhanced photoacoustic spectroscopy (QEPAS) was demonstrated as an alternative way to detect the photoacoustic signal in 2002 [17]. Standard watch QTFs with a resonance frequency of 32,768 (i.e., 2^{15}) Hz are typically employed as acoustic transducers instead of microphones and cantilevers, due to their high Q factor, compactness, and low cost [18–27]. These QTFs show ultra-narrow acoustic response widths of a few Hz in a quadrupole configuration, thus providing a strong environmental noise immunity [28,29]. Acoustic micro-resonators (AmR) made of stainless-steel pipes or capillary tubes can be coupled with QTFs, creating acoustic resonances, and enhancing the PA signal-to-noise ratio [30]. A QTF coupled with an AmR constitutes a QEPAS spectrophone and in the past decades, various types of QEPAS spectrophones have been developed to boost the QEPAS sensor performance [31–35].

However, QEPAS spectrophones face problems in the employment of sources characterized by poor beam profile qualities such as LEDs, fiber-amplified lasers, and QCL THz sources. When implementing standard watch QTFs for QEPAS, the light beam must pass through the 200–300-μm prong spacing and the AmR (typically ~1-cm long) without hitting them. Any light illuminating the QTF prongs and AmR walls will generate photothermal background noise and scattered light noise, strongly decreasing the sensor signal-to-noise ratio [36–38]. In 2013, the use of a custom QTF was proposed for QEPAS sensing for

the first time, which is characterized by a large prong spacing (1 mm) by coupling it with a THz QCL source [39]. A review of custom QTFs for photoacoustic gas sensing is provided in Ref. [40]. In 2018, the second generation of custom tuning forks was proposed with improved geometry and prongs spacing up to 1.5 mm, T-shaped longitudinal cross section, and grooved prong surfaces [41]. Custom QTFs for photoacoustic gas sensing have also been demonstrated by Duquesnoy [42], Ma [43], and Zheng [10,44], as well as others. QEPAS configurations such as intracavity enhancement, overtone resonance, single-tube on-beam configuration, double antinode excitation, in-plane excitation, and multiple-sound-source excitation were demonstrated by exploiting custom QTFs [15,45]. A few samples of these custom QTFs were manufactured through a series of physical and chemical processes, including quartz substrate metallization, photoresist deposition, UV exposure, and metal etching. As a result, custom QTFs can cost up to a few thousands of dollars, much more than watch QTFs that, thanks to their large industrial production, are available at a very low cost (~10 cents).

In this work, we introduce an effective method to manufacture a clamp-type custom QTF starting from a watch QTF for photoacoustic gas sensing.

The schematics of the clamp-type QTF and corresponding spectrophone are shown in Fig. 1. The aperture diameter d, prong length l_1, QTF length l_2, prong width w, and QTF thickness t are also denoted in Fig. 1(a). A circular aperture was carved out from the QTF to facilitate the light beam transmission. Finite element analysis was performed by the "Pressure Acoustic, Frequency Domain" module of COMSOL Multiphysics to analyze the resonance frequency dependence on aperture diameters. The QTF can be modeled as a cantilever beam with one end fixed that vibrates in a flexural mode, as shown in Fig. 2(a). According to the laser excitation position effect, the circle aperture center was fixed 0.7 mm below the QTF top, corresponding to the optimal focal position for QEPAS sensing with standard watch QTFs [30]. The l_1, l_2, w, and t are set as 3.8 mm, 6 mm, 0.6 mm, and 0.3 mm, respectively. With the aperture diameters varying from 500 μm to 1000 μm, the resonance frequencies of the clamp-type QTF are predicted to increase from 33,023 Hz to 37,382 Hz, as shown in Fig. 2(b). A polynomial function was employed to fit the curve and obtain the following empirical equation:

$$f_{th} = 33349.571 - 5.251d + 0.00925d^2, \quad \textbf{(1)}$$

where f_{th} is the theoretical resonance frequency and d is the aperture diameter of the clamp-type QTF.

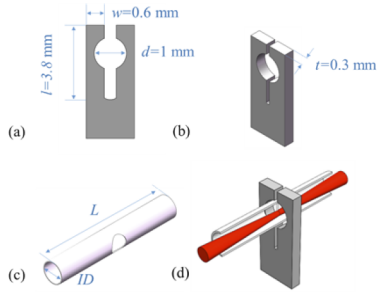

Fig. 1. (a) Front view of a clamp-type QTF. (b) Isometric diagram of a clamp-type QTF. (c) Diagram of single-tube longitudinal AmR. (d) Section view of clamp-type SO-QEPAS spectrophone.

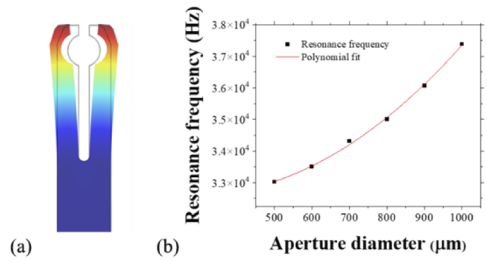

Fig. 2. (a) Finite element analysis of the vibration of clamp-type QTF. (b) QTF resonance frequencies as the function of aperture diameters.

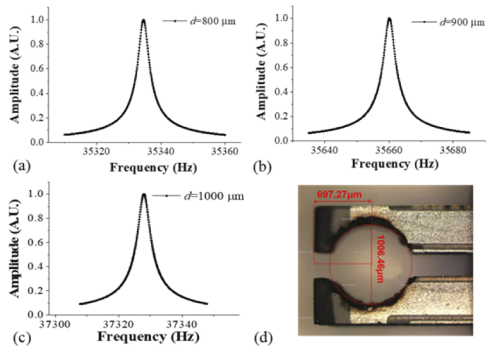

Fig. 3. (a)–(c) Resonance curves for clamped QTFs with an aperture diameter of 800 μm, 900 μm, and 1 mm, respectively. (d) Photograph of the clamp-type QTF with 1-mm aperture.

Wet chemical etching for 120 min was carried out by using 40% hydrofluoric acid at room temperature and atmospheric pressure. A custom polytetrafluoroethylene (PTFE) mask with a round hole was used to control the etched spacing shape. Clamp-type QTFs with circle aperture diameters from ~800 μm to ~1 mm were obtained.

Resonance curves of the clamp-type QTFs were measured and are shown in Fig. 3. Lorentzian-like functions were used to fit the data points. The resonance frequencies f_{ex} for apertures of $d = 800$ μm, 900 μm, and 1000 μm were 35,334 Hz, 35,660 Hz, and 37,327 Hz, respectively, in good agreement with theoretical predictions. Figure 3(d) shows the picture of a clamp-type QTF with a ~1-mm circle aperture. The Q factors of all clamp-type QTFs reached a value higher than 10,000. Detailed values of Q and f_{ex} are summarized in Table 1. The experimental results show the same trend with the aperture diameter predicted by the theoretical analysis, i.e., resonance frequency increases with the aperture diameter. This is mainly due to the reduction in the QTF mass with increasing the aperture size. The slight discrepancy between theoretical and experimental f_{ex} values comes from irregularities in the shape of the etched aperture. A 10.6-μm laser cutting system was used to modify the irregularities, achieving a more regular circular aperture, as shown in Fig. 3(d). Compared with a standard watch QTFs, the area is more than ten times larger, thereby making this clamp-type QTFs an attractive choice when operating with a laser source characterized by a low-quality beam profile.

To verify the possibility to implement a micro-resonator system for clamp-type QTFs, a single-tube on-beam resonator spectrophone (SO-QEPAS) was realized. The SO-QEPAS configuration can effectively enhance the spectrophone sensitivity

Table 1. Parameters of Three Clamp-Type QTFs[a]

Length l_1/mm	Width w/mm	Aperture d/mm	f_{th}/Hz	f_{ex}/Hz	Q Factor
3.8	0.6	0.8	35,005	35,334	11,325
		0.9	36,068	35,660	10,582
		1.0	37,382	37,327	10,098

[a] f_{th}, theoretical frequency; f_{ex}, experimental frequency.

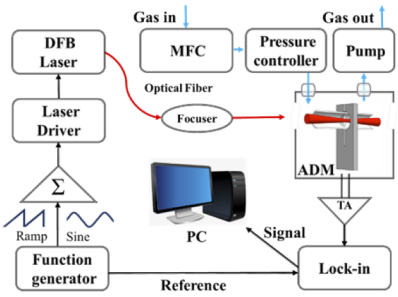

Fig. 4. Schematic diagram of the clamp-type quartz tuning fork enhanced photoacoustic spectroscopy setup. MFC, mass flow controller; ADM, acoustic detection module; TA, transimpedance amplifier; Σ, adder; PC, personal computer.

while keeping the resonator tube length shorter when compared with a dual tube configuration. The SO-QEPAS configuration is not feasible for a standard watch QTF due to its low prong spacing (200–300 μm) [46]. As a compromise between the resonance frequency and Q factor, a clamp-type QTF with an aperture diameter of 900 μm was selected. Considering the wall thickness of ~0.1 mm, a set of single-tube AmRs with an inner diameter (ID) from 0.4 to 0.6 mm was realized. A pilot hole with a diameter of ~300 μm was made in the middle of a stainless-steel capillary, forming a longitudinal AmR, as shown in Fig. 1(c). The hole diameter is comparable with the QTF thickness t, thereby with the expectation to provide a maximum acoustic coupling effect. The AmR was inserted through the clamp-type aperture perpendicularly to the QTF plane, realizing a SO-QEPAS configuration, as schematically shown in Fig. 1(d).

The schematic diagram of the clamp-type quartz tuning fork enhanced photoacoustic spectroscopy setup is shown in Fig. 4. As proof of concept, a 1.39-μm near-infrared DFB laser was employed as the excitation source to detect water vapor in the air to demonstrate the clamp-type QEPAS sensor operation. The output laser beam from the DFB laser was collimated through the ~0.9-mm aperture of the clamp-type QTF by an optical fiber focuser (OZ Optics). A single-tube AmR was inserted in the circular aperture of the clamp QTF. According to one-dimensional longitudinal resonator theory, the optimum AmR length L should be in the range of $\lambda/4 < L < \lambda/2$, where λ is the wavelength of the sound wave. Modulation and tuning of the laser current were controlled by applying a sinusoidal dither to the direct current ramp. The sinusoidal dither was set at half of the QTF resonance frequency f_{ex}. The piezoelectric signal generated by the QTF was pre-processed by a low noise transimpedance amplifier (TA) with a 10-MΩ feedback resistor. A lock-in amplifier (Stanford Research System, SR830 DSP) was used for second harmonic demodulation with 1-s integration time and 12-dB/Oct slope. Mass flow controller, pressure controller, pump, and valves were used to set the air gas flow to

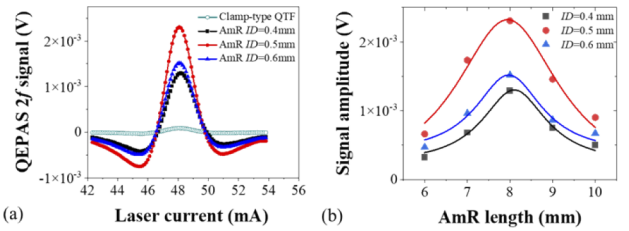

Fig. 5. (a) $2f$ signals obtained by the clamp-type SO-QEPAS spectrophone for different inner diameters (IDs) of the AmR. (b) QEPAS signal amplitude as the function of AmR length for different IDs.

100 standard cubic centimeters per minute (SCCM) and keep the pressure constant.

Figure 5(a) depicts the $2f$ signals obtained by three different clamp-type SO-QEPAS spectrophones with AmR ID of 0.4 mm, 0.5 mm, and 0.6 mm, respectively. The AmR length of all the clamp-type SO-QEPAS spectrophones was set at 8 mm. According to one-dimensional longitudinal resonator theory [30], the overall optimum AmR length should be between 4.75 mm ($\lambda/2$) and 9.5 mm (λ). The exact optimum value should be determined by experiment. In Fig. 5(b), the AmR length was changed from 6 mm to 10 mm with the step size of 1 mm. With an optimized AmR length of 8 mm and ID of 0.5 mm, the clamp-type SO-QEPAS spectrophone shows a maximum signal amplitude of 2.35×10^{-3}, which is ~30 times larger than the one measured for a bare clamp-type QTF (~8×10^{-5} V). The obtained 1σ noise levels are comparable, ~1.2×10^{-6} V. Compared with the optimal size of the standard watch QEPAS spectrophone, the optimal longitudinal resonator length was reduced by ~20%. Considering a water vapor concentration of 15,000 ppm and a 1σ noise level of 1.2×10^{-6} V, the signal-to-noise ratio (SNR) was ~1940. Consequently, a normalized noise equivalent absorption (NNEA) coefficient of 1.78×10^{-8} W/cm/Hz$^{1/2}$ was achieved.

In conclusion, we reported on the design, realization, and optimization of clamp-type QTFs for photoacoustic gas sensing. The clamp-type QTFs can be manufactured based on cost-effective watch QTFs with only one step, achieving a quite cost-effective way for obtaining custom QTFs. The clamp-type QTF provides an increase of the area between the prong available for light beam accommodation of more than 10 times with respect to a standard watch QTF, while still providing Q factors > 10^4. This large aperture of clamp-type QTFs opens the way to their applications with light sources having poor beam quality such as high-power LEDs or THz QCLs sources. Compared with a previously reported U-shaped custom QTF, the wavefront shape of the clamp-type QTF helps to improve the acoustic wave coupling efficiency. The possibility to implement a micro-resonator system for clamp-type QTFs was also investigated. A ~30 times signal-to-noise enhancement has been achieved with an optimal single-tube AmR length of 8 mm, compared with a bare clamp-type QTF. The AmR was ~20% less than the optimal dual-tube AmR employed for the standard watch QTF, thereby demonstrating the advantage of implementing clamp-type QTFs even with laser sources with good beam profile such as near-IR diode lasers.

Further improvements can be achieved by exploiting the clamp-type approach to standard QTF geometries and these results could be beneficial also for tuning fork photodetection performance [47–52] and QTF-based atomic force microscopy.

More sophisticated technology such as femtosecond laser micromachining and numerical control machine tool can be used to polish a desired shape for the QTF.

Funding. National Key Research and Development Program of China (2021YFB2800801,2019YFE0118200); National Natural Science Foundation of China (12174156, 12174155, 62105125, 62005105, 62075088, 62175137); Natural Science Foundation of Guangdong Province (2020B1515020024, 2019A1515011380); Science and Technology Projects of Guangzhou (202102020445); Key-Area Research and Development Program of Guangdong Province (2019B010138004); Project of Guangzhou Industry Leading Talents (CXLJTD-201607); Chinese Aeronautical Establishment (201808W4001); Special Project in Key Fields of the Higher Education Institutions of Guangdong Province (2020ZDZX3022); Open Foundation of CEPREI (No. 19D09); Foundation for Distinguished Young Talents in Higher Education of Guangdong (2018KQNCX009); Fundamental Research Funds for the Central Universities (21619402, 11618413); State Key Laboratory of Applied Optics (SKLAO-201914).

Disclosures. The authors declare no conflicts of interest.

Data availability. Data underlying the results presented in this paper are not publicly available at this time but may be obtained from the authors upon reasonable request.

Supplemental document. See Supplement 1 for supporting content.

REFERENCES

1. S. Qiao, Y. He, and Y. Ma, Opt. Lett. **46**, 2449 (2021).
2. J. Karhu, T. Tomberg, F. S. Vieira, G. Genoud, V. Hänninen, M. Vainio, M. Metsälä, T. Hieta, S. Bell, and L. Halonen, Opt. Lett. **44**, 1142 (2019).
3. A. Sampaolo, P. Patimisco, M. Giglio, A. Zifarelli, H. Wu, L. Dong, and V. Spagnolo, Anal. Chim. Acta **1202**, 338894 (2022).
4. G. Yang, H. Huang, H. Luo, S. Kou, E. Amidi, S. Achilefu, and Q. Zhu, Opt. Lett. **46**, 2706 (2021).
5. K. Chamassi, W. Trzpil, R. Arinero, R. Rousseau, A. Vicet, and M. Bahriz, Appl. Phys. Lett. **115**, 081106 (2019).
6. K. Chen, B. Yang, M. Guo, H. Deng, B. Zhang, S. Liu, C. Li, R. An, W. Peng, and Q. Yu, Opt. Lett. **45**, 2458 (2020).
7. L. Liu, A. Mandelis, H. Huan, and K. H. Michaelian, Opt. Lett. **42**, 1424 (2017).
8. W. Trzpil, J. Charensol, D. Ayache, N. Maurin, R. Rousseau, A. Vicet, and M. Bahriz, Sens. Actuators, B **353**, 131070 (2022).
9. S. Zhou and D. Lannuzzi, Rev. Sci. Instrum. **90**, 023102 (2019).
10. H. Lin, H. Zheng, B. A. Zhou Montano, H. Wu, M. Giglio, A. Sampaolo, P. Patimisco, W. Zhu, Y. Zhong, L. Dong, R. Kan, J. Yu, and V. Spagnolo, Photoacoustics **25**, 100321 (2022).
11. J. Hass and B. Mizaikoff, Annual Rev. Anal. Chem. **9**, 45 (2016).
12. C. S. Liao, R. Blanchard, C. Pfluegl, M. Azimi, F. Huettig, and D. Vakhshoori, Opt. Lett. **45**, 3248 (2020).
13. J. Karhu, H. Philip, A. Baranov, R. Teissier, and T. Hieta, Opt. Lett. **45**, 5962 (2020).
14. T. Tomberg, M. Vainio, T. Hieta, and L. Halonen, Sci. Rep. **8**, 1848 (2018).
15. P. Patimisco, A. Sampaolo, L. Dong, F. K. Tittel, and V. Spagnolo, Appl. Phys. Rev. **5**, 011106 (2018).
16. Z. Wang, H. Wei, Y. Li, R. Kan, and W. Ren, Opt. Lett. **45**, 1148 (2020).
17. A. A. Kosterev, Y. A. Bakhirkin, R. F. Curl, and F. K. Tittel, Opt. Lett. **27**, 1902 (2002).
18. Q. Wang, Z. Wang, W. Ren, P. Patimisco, A. Sampaolo, and V. Spagnolo, Sens. Actuators, B **268**, 512 (2018).
19. M. Duquesnoy, G. Aoust, J. M. Melkonian, R. Levy, M. Raybaut, and A. Godard, Appl. Phys. B **127**, 150 (2021).
20. Y. Ma, Y. Hong, S. Qiao, Z. Lang, and X. Liu, Opt. Lett. **47**, 601 (2022).
21. R. Rousseau, Z. Loghmari, M. Bahriz, K. Chamassi, R. Teissier, A. N. Baranov, and A. Vicet, Opt. Express **27**, 7435 (2019).
22. J. P. Waclawek, H. Moser, and B. Lendl, Opt. Express **24**, 6559 (2016).
23. R. Lewicki, G. Wysocki, A. A. Kosterev, and F. K. Tittel, Opt. Express **15**, 7357 (2007).
24. L. Xu, N. Liu, S. Zhou, L. Zhang, B. Yu, H. Fischer, and J. Li, Opt. Express **28**, 5648 (2020).
25. Z. Wang, C. Tian, S. Qian, Y. Yu, J. Chang, Q. Zhang, Y. Feng, H. Li, and Z. Feng, Opt. Laser Technol. **145**, 107483 (2022).
26. L. Dong, J. Wright, B. Peters, B. A. Ferguson, F. K. Tittel, and S. McWhorter, Appl. Phys. B **107**, 459 (2012).
27. C. Lin, Y. Liao, and F. Fang, Appl. Spectrosc. **73**, 000370281986646 (2019).
28. H. Wu, L. Dong, H. Zheng, Y. Yu, W. Ma, L. Zhang, W. Yin, L. Xiao, S. Jia, and F. K. Tittel, Nat. Commun. **8**, 15331 (2017).
29. T. Rück, R. Bierl, and F. M. Matysik, Sens. Actuators, B **255**, 2462 (2018).
30. H. Zheng, L. Dong, H. Wu, X. Yin, L. Xiao, S. Jia, R. F. Curl, and F. K. Tittel, Chem. Phys. Lett. **691**, 462 (2018).
31. L. Dong, A. A. Kosterev, D. Thomazy, and F. K. Tittel, Appl. Phys. B **100**, 627 (2010).
32. K. Liu, X. Guo, H. Yi, W. Chen, W. Zhang, and X. Gao, Opt. Lett. **34**, 1594 (2009).
33. L. Hu, C. Zheng, J. Zheng, Y. Wang, and F. K. Tittel, Opt. Lett. **44**, 2562 (2019).
34. H. Lv, H. Zheng, Y. Liu, Z. Yang, Q. Wu, H. Lin, B. A. Zhou Montano, W. Zhu, J. Yu, R. Kan, Z. Chen, and F. K. Tittel, Opt. Lett. **46**, 3917 (2021).
35. H. Zheng, L. Dong, A. Sampaolo, H. Wu, P. Patimisco, X. Yin, W. Ma, L. Zhang, W. Yin, V. Spagnolo, S. Jia, and F. K. Tittel, Opt. Lett. **41**, 978 (2016).
36. H. Zheng, L. Dong, X. Yin, X. Liu, H. Wu, L. Zhang, W. Ma, W. Yin, and S. Jia, Sens. Actuators, B **208**, 173 (2015).
37. Y. Ma, R. Lewicki, M. Razeghi, and F. K. Tittel, Opt. Express **21**, 1008 (2013).
38. M. Helman, H. Moser, A. Dudkowiak, and B. Lendl, Appl. Phys. B **123**, 141 (2017).
39. S. Borri, P. Patimisco, A. Sampaolo, H. E. Beere, D. A. Ritchie, M. S. Vitiello, G. Scamarcio, and V. Spagnolo, Appl. Phys. Lett. **103**, 021105 (2013).
40. P. Patimisco, A. Sampaolo, H. Zheng, L. Dong, F. K. Tittel, and V. Spagnolo, Adv. Phys.: X **2**, 169 (2017).
41. P. Patimisco, A. Sampaolo, M. Giglio, S. Dello Russo, V. Mackowiak, H. Rossmadl, A. Cable, F. K. Tittel, and V. Spagnolo, Opt. Express **27**, 1401 (2019).
42. M. Duquesnoy, G. Aoust, J. M. Melkonian, R. Levy, M. Raybaut, and A. Godarad, Sensors **19**, 1362 (2019).
43. Y. Ma, Y. He, P. Patimisco, A. Sampaolo, S. Qiao, X. Yu, F. K. Tittel, and V. Spagnolo, Appl. Phys. Lett. **116**, 011103 (2020).
44. H. Zheng, Y. Liu, H. Lin, B. Liu, D. Li, B. Huang, Y. Wu, L. Dong, W. Zhu, J. Tang, H. Guan, H. Lu, Y. Zhong, J. Fang, Y. Luo, J. Zhang, J. Yu, and F. K. Tittel, Photoacoustics **17**, 100158 (2020).
45. R. Cui, H. Wu, L. Dong, W. Chen, and F. K. Tittel, Appl. Phys. Lett. **118**, 161101 (2021).
46. H. Zheng, L. Dong, A. Sampaolo, P. Patimisco, W. Ma, L. Zhang, W. Yin, L. Xiao, V. Spagnolo, S. Jia, and F. K. Tittel, Appl. Phys. Lett. **109**, 111103 (2016).
47. Y. F. Ma, Y. He, Y. Tong, X. Yu, and F. K. Tittel, Opt. Express **26**, 32103 (2018).
48. T. Wei, A. Zifarelli, S. Dello Russo, H. Wu, G. Menduni, P. Patimisco, A. Sampaolo, V. Spagnolo, and L. Dong, Appl. Phys. Rev. **8**, 041409 (2021).
49. Y. Liu, H. Lin, B. A. Zhou Montano, W. Zhu, Y. Zhong, R. Kan, B. Yuan, J. Yu, M. Shao, and H. Zheng, Photoacoustics **25**, 100332 (2022).
50. Z. Shang, H. Wu, S. Li, F. K. Tittel, and L. Dong, Appl. Phys. Lett. **120**, 171101 (2022).
51. Z. Lang, S. Qiao, and Y. Ma, Opt. Lett. **47**, 1295 (2022).
52. Y. Ma, W. Feng, S. Qiao, Z. Zhao, S. Gao, and Y. Wang, Opt. Express **30**, 18836 (2022).